



OPEN

First-principles Dzyaloshinskii–Moriya interaction in a non-collinear framework

R. Cardias^{1,2,3✉}, A. Szilva², M. M. Bezerra-Neto⁴, M. S. Ribeiro⁵, A. Bergman², Y. O. Kvashnin², J. Fransson², A. B. Klautau¹, O. Eriksson^{2,6} & L. Nordström²

We have derived an expression of the Dzyaloshinskii–Moriya interaction (DMI), where all the three components of the DMI vector can be calculated independently, for a general, non-collinear magnetic configuration. The formalism is implemented in a real space—linear muffin-tin orbital—atomic sphere approximation (RS-LMTO-ASA) method. We have chosen the Cr triangular trimer on Au(111) and Mn triangular trimers on Ag(111) and Au(111) surfaces as numerical examples. The results show that the DMI (module and direction) is drastically different between collinear and non-collinear states. Based on the relation between the spin and charge currents flowing in the system and their coupling to the non-collinear magnetic configuration of the triangular trimer, we demonstrate that the DMI interaction can be significant, even in the absence of spin-orbit coupling. This is shown to emanate from the non-collinear magnetic structure, that can induce significant spin and charge currents even with spin-orbit coupling is ignored.

Chiral objects are unique and present intriguing properties. In the field of magnetism, topologically quantized magnetic whirl textures, called Skyrmions, have been widely explored in literature^{1–9}. Due to its topological protection, the skyrmion is regarded as a novel particle with potential applicability in information technology. Chiral magnets are characterized by the presence of the Dzyaloshinskii–Moriya interaction (DMI)^{10–12}, which results from spin-orbit coupling (SOC) combined with absence of inversion symmetry¹¹. Both strength and direction of the DMI have been reported^{13–15}, where the latter is known due to symmetry reasons for the cases of bulk, surfaces and even impurities on surfaces; but to calculate the DMI for nanostructures with low symmetry is still a challenge.

Several methods in the literature are used to study static and dynamical properties of magnetic materials, such as magnetic ground state, phase transition, critical temperature, magnetic dynamics etc. In order to achieve that, spin-Hamiltonians can be used to model the system and calculate these properties^{16–24}. In the simple case of a bi-linear spin-Hamiltonian, both exchange-coupling parameter J_{ij} and the DMI are needed to correctly describe the studied system, and a common expression is

$$E = - \sum_{i \neq j} J_{ij} \mathbf{e}_i \cdot \mathbf{e}_j - \sum_{i \neq j} \mathbf{D}_{ij} \cdot (\mathbf{e}_i \times \mathbf{e}_j). \quad (1)$$

In this expression \mathbf{e}_i represents the direction of the magnetic moment at site i , and the sum is done over pairs of spins. The interatomic exchange interaction between spins is J_{ij} , and theoretical calculations of it and the DMI, \mathbf{D}_{ij} , offers the possibility to predict important properties, e.g. magnon excitations¹⁶, which are important for fields such as spintronics and its technological applications. However, it was shown that these parameters are strongly affected by non-collinearity in case of non-Heisenberg systems²⁵ and, therefore, the properties need to be calculated under a non-collinear formalism. In fact, it has been shown that the calculation of magnon excitations in bcc Fe are closer to the experimental results if one takes into account the calculation of J_{ij} in the non-collinear (NC) framework²⁶. Furthermore, in more complex systems, DMI can play an important role in the magnon spectra calculation^{23,27}. Also, as the systems get more and more complex, the magnetic structure needs to be taken into consideration for a more precise description of the static and dynamic properties. For that, specifically for

¹Faculdade de Física, Universidade Federal do Pará, Belém, PA, Brazil. ²Department of Physics and Astronomy, Uppsala University, Box 516, 75120 Uppsala, Sweden. ³SPEC, CEA, CNRS, Université Paris-Saclay, CEA Saclay, 91191, Gif-sur-Yvette, France. ⁴Instituto de Engenharia e Geociências, Universidade Federal do Oeste do Pará, Santarém, PA, Brazil. ⁵Instituto Federal do Pará, Campus Belém, Belém, PA, Brazil. ⁶School of Science and Technology, Örebro University, 701 82 Örebro, Sweden. ✉email: ramon.cardias@cea.fr

the DMI, a NC description is needed. In this work, we show that the DMI is quite different, both regarding the strength and direction, for different magnetic configurations. For instance, for triangular trimers considered in this work, where there is a local minima at the Néel configuration (in-plane magnetic moments with an angle of 120° between each other), the DMI is different in direction and strength compared with the DMI calculated considering a collinear configuration. Similar to what the improved J_{ij} could provide in Ref.²⁶, we believe that a general expression for the DMI can lead to new and better understanding of experimental nano-magnetism.

In the absence of SOC interaction, the interatomic exchange coupling can be mapped onto a scalar Heisenberg spin model derived in terms of infinitesimal spin rotations based on Green's function formalism that is known as the Liechtenstein-Katsnelson-Antropov-Gubanov (LKAG) formalism²⁸. The method has been extended for NC atomistic spin configurations in Ref.²⁶. Here, we present a calculation method for the DMI vectors when the SOC is present as a perturbation resulting in (only) anti-symmetric off-diagonal elements of the exchange tensor. This method has two advantages. Firstly, it may give an efficient and expedient estimation for the DMI vectors from a computational point of view. Secondly, this method is able to handle NC atomistic spin configuration by having explicit formulas for the three components for the DMI vectors in the NC framework²⁶. We describe here the implementation of this method and illustrate its applicability on selected magnetic nano-sized objects. In order to reach the established goals, we used the linear muffin-tin orbital—atomic sphere approximation method (RS-LMTO-ASA) to calculate self-consistently the electronic structure for each studied structure.

We have considered Cr triangular trimer supported on the Au(111) surface (Cr₃/Au(111)) and Mn triangular trimers supported on the Ag(111) (Mn₃/Ag(111)) and Au(111) (Mn₃/Au(111)) surfaces. As described in the “Methods” section, we have employed a linear muffin-tin orbital method in the atomic sphere approximation for the calculation of the electronic structure. Furthermore we considered a real-space version of this method, which enables calculations without periodic boundary conditions, such as clusters of atoms on a substrate. The fcc(111) substrate has been modeled by a slab of 4500 atoms with the experimental lattice parameter of Au (or Ag). To simulate the vacuum, outside the surface, we added two layers of empty spheres above the Ag (or Au) surface, in order to provide a basis for the wave function in the vacuum and to treat charge transfers correctly. The calculations of the Mn (or Cr) adsorbed clusters have been performed by embedding the clusters as a perturbation on the previously self-consistently converged Au(111) or Ag(111) surfaces. The Mn (Cr) sites and the first-nearest-neighbor (NN) atoms (Ag or Au, and empty spheres) around the defect were recalculated self-consistently, while the electronic structure for atoms far from the Mn (Cr) cluster were kept unchanged. The collinear and the NC solutions presented here were obtained from fully relativistic calculations, where the spin-orbit interaction was treated at each variational step²⁹. We have performed calculations without structural relaxation, where the Mn (Cr) atoms occupy the unrelaxed hollow positions, assuming the experimental lattice parameter of the Ag (or Au) substrate. The DMI parameters, D_{ij} 's, have been computed using an implementation following the theory described in Ref.²⁶ and further details are shown in the next section. The obtained values of D_{ij} are then used to analyse the effects of non-collinearity onto its strength and direction, aiming to show their differences and consequently their importance for further studies that use them.

Spin interactions

Let us consider a system that is described by the spin Hamiltonian given by Eq. (1). If a spin at site i is rotated by infinitesimally small angles and the rest of the spins are unperturbed then an energy variation term, δE_i can be calculated. In the case when two spins in the spin system at site i and j are simultaneously rotated by infinitesimally small angles and the rest of the spins are unperturbed then the total energy variation is given as

$$\delta E = \delta E_i + \delta E_j + \delta E_{ij}, \quad (2)$$

where the last term characterizes the interaction between the two spins while the other first two terms describe the interaction with the rest of spin system. We will focus on the interacting term δE_{ij} which is given as

$$\delta E_{ij} = -2J_{ij}\delta\mathbf{e}_i\delta\mathbf{e}_j - 2\mathbf{D}_{ij}(\delta\mathbf{e}_i \times \delta\mathbf{e}_j). \quad (3)$$

The reason we do it is that the same scheme can be applied for the electronic grand potential variation, $\delta\Omega$, under the same perturbation. It will have also three terms when two spins are simultaneously rotated by infinitesimally small angles at the same time. The analog interacting term is denoted by $\delta\Omega_{ij}$. For this terms we have derived an expression in terms of multiple scattering electronic structure theory, see Eq. (19) in the “Methods” section. Having Eq. (19), it is easy to identify $-2J_{ij}\delta\mathbf{e}_i\delta\mathbf{e}_j$ and $-2\mathbf{D}_{ij}(\delta\mathbf{e}_i \times \delta\mathbf{e}_j)$ in Eq. (3) with $-2J_{ij}^*\delta\mathbf{e}_i\delta\mathbf{e}_j$ and $-2\mathbf{D}_{ij}^*(\delta\mathbf{e}_i \times \delta\mathbf{e}_j)$, respectively. In other words, the Heisenberg exchange parameter, J_{ij} can be mapped onto an expression that contains information from the electronic structure, J_{ij}^* , defined by Eq. (20) in the “Methods” section. Expression J_{ij}^* is reduced to (Eq. (22)) in the collinear limit, which is commonly referred to as the LKAG formula. On the top of this, \mathbf{D}_{ij} of the spin-Hamiltonian can be mapped onto information of the electronic structure energy, represented by \mathbf{D}_{ij}^* in Eq. (21) of the “Methods” section. This expression is derived for the general, NC, spin-alignment. The corresponding expressions for the DMI in the collinear limit were obtained in Refs.^{30,31}. We show in the “Methods” section that the presence of SOC interaction mainly contribute to $-2\mathbf{D}_{ij}^*(\delta\mathbf{e}_i \times \delta\mathbf{e}_j)$, see Eq. (37).

We note that the derivation of how to calculate the J_{ij} and \mathbf{D}_{ij} parameters from the electronic structure is based on the analysis of two-site energy variation, i.e, the mapping procedure is here made by the comparison of δE_{ij} to $\delta\Omega_{ij}$. It should be also noted that the exchange and DMI parameters in Ref.³² have been derived from one-spin rotation when the application of the NC, generalized, LKAG sum rule makes possible to make a mapping between electronic structure properties and an effective spin-Hamiltonian. This approach was also shown in Ref.³³. The detailed presentation of the connection of the two approaches will be the part of a further study.

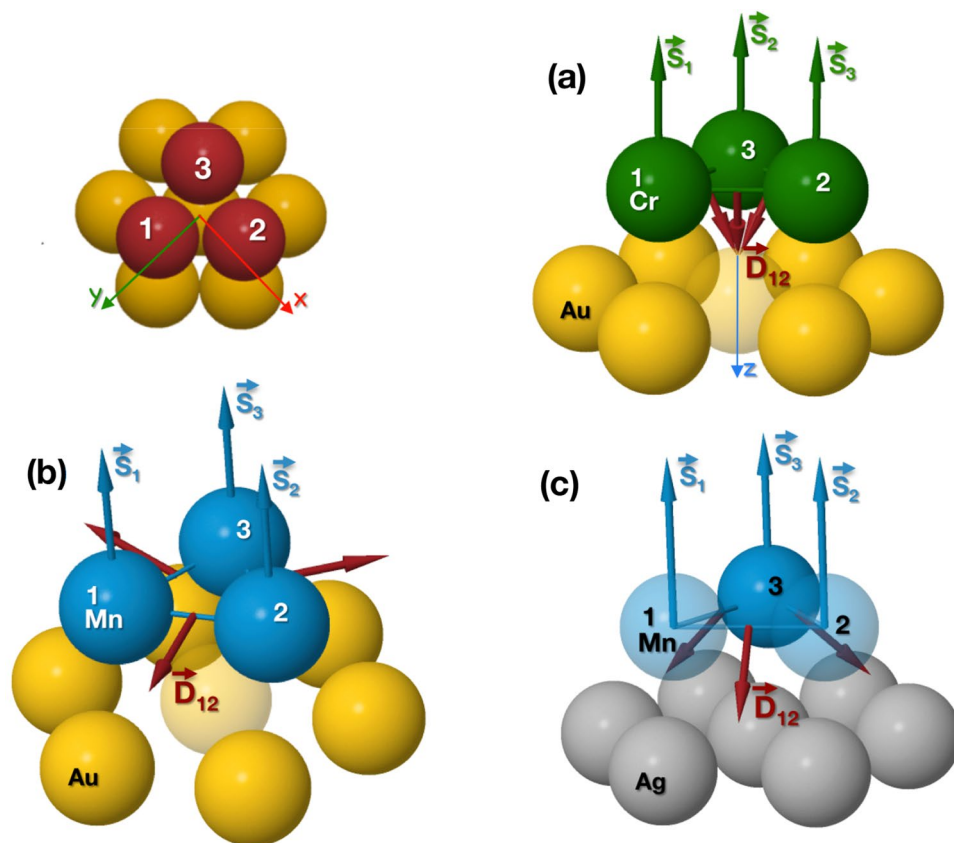


Figure 1. Schematic representation of a triangular trimer on an fcc substrate (top left) and the adopted coordinate system. In (a) the moments and DMI vectors of Cr on Au(111) are shown. In (b) results for Mn on fcc Au(111) are displayed, and in (c) results for Mn on fcc Ag(111) is shown. The dark red arrows denote the DMI direction (\mathbf{D}_{ij}), calculated for a collinear magnetic configuration (ferromagnetic with the magnetic moments ($\mathbf{S}_1, \mathbf{S}_2, \mathbf{S}_3$) perpendicular to the surface along $-\hat{z}$).

	D_{\parallel}	D_z
(a) Cr on Au(111)	-1.51	2.77
(b) Mn on Au(111)	1.68	-0.04
(c) Mn on Ag(111)	1.01	0.96

Table 1. The strength of the in-plane and out-of-plane components of the DMI vector, in meV. Note that (a), (b) and (c) denotes the systems shown in Fig. 1 of a triangular trimer of Cr on Au(111) surface, Mn on Au(111) and Ag(111) surfaces, respectively. The DMI calculations were performed for magnetic moments in a ferromagnetic configuration, with the magnetic moments pointing perpendicular to the surface.

Lastly, in Ref.¹¹ the derivative of the free energy up to the second order with respect to the angle is used as a different approach to calculate the DMI.

Numerical results

Cluster geometry and collinear DMI. In order to test the formalism presented here, we investigate the simple case of a triangular trimer of: (a) Cr on Au(111), Mn on (b) Au(111) and (c) Ag(111) fcc surfaces, considering a collinear magnetic configuration with the atomic moments perpendicular to the surface. For all three cases, the three DMI directions are all related by the C_{3v} symmetry of the triangle trimer, and hence in accordance to what is expected by Moriya's rules¹³ and the surface symmetry. Although, one can see in Fig. 1 that their in-plane and out-of-plane components point to different direction. Concerning their strength, the values are listed in Table 1. The DMI values are calculated between atoms 1 and 2 (see Fig. 1) and, in this particular coordinate system, this DMI vector has two independent components, an in-plane and an out-of-plane, $\mathbf{D}_{12} = D_{\parallel} \hat{n} + D_z \hat{z}$, with $\hat{n} = (\hat{x} + \hat{y})/\sqrt{2}$.

Note that DMI for the Mn trimer on Ag(111) is comparable with the one of the Mn trimer on Au(111), despite the fact that Au has a larger spin-orbit coupling than Ag. One would therefore expect that an interaction

	$ D_{ij} _{\text{collinear}}$	$ D_{ij} _{\text{CP}}$
(a) Cr on Au(111)	3.16	133.62
(b) Mn on Au(111)	1.68	81.74
(c) Mn on Ag(111)	1.40	59.83

Table 2. Comparison of the strength of the DMI between the collinear and CP configuration, in meV. Note that (a), (b) and (c) denotes the systems shown in Fig. 1 of a triangular trimer of Cr on Au(111) surface, Mn on Au(111) and Ag(111) surfaces, respectively.

that commonly is ascribed to pure spin-orbit effects, would be larger for the latter substrate. However, the Au 5*d* bands hybridize only weakly with the 3*d* states of Mn³⁴. This weakens the influence of the large spin-orbit coupling of the Au atom. In contrast, the hybridization between Mn and Ag is stronger. Although Ag has a weaker spin-orbit strength compared to Au, this increase in hybridization results in a DM interaction that is similar for the two systems.

If one considers the Heisenberg Hamiltonian for the triangular trimer, for systems where the J_{ij} favours anti-ferromagnetism, which is the case for all of the systems studied here, the magnetic configuration that minimizes the equation is the known Néel configuration, where the magnetic moments are in-plane with an angle of 120° between each other. In that case, the D_z component is responsible to lift the degeneracy between different signs of the vector chirality $\chi = \mathbf{S}_1 \times \mathbf{S}_2 + \mathbf{S}_2 \times \mathbf{S}_3 + \mathbf{S}_3 \times \mathbf{S}_1$ in the Néel configuration¹⁴. It has been discussed in Ref.²⁶ that the Heisenberg picture can be broken and non-Heisenberg quantities can play an important role in case of non-collinearity, therefore changing the values of J_{ij} and \mathbf{D}_{ij} . In the next section, we show that the calculated DMI's highly depend on their magnetic configuration reference by calculating the DMI's for their respective NC, minima.

Non-collinear DMI. At this stage of the calculation, the magnetic moments were allowed to relax in orientation, to find the lowest energy configuration. The co-planar 120° Néel state was found to be the local minimum energy configuration. For this co-planar (CP) configuration, the Heisenberg exchange and DMI interaction were calculated, according to the discussion of the previous section and the “Methods” section. The results were significantly different, both in direction and strength, compared to the ones found for the collinear case. In the CP case, all three studied systems have the DMI direction almost exclusively perpendicular to the surface, with the in-plane components D_x and D_y being very weak compared with D_z . The strengths of these DM interactions are quite intriguing, since they are approximately one order of magnitude larger than the strength of the collinear case. A similar behaviour was discussed in Ref.³² for the compound Mn₃Sn. It is important to mention that in Ref.³², the J_{ij} 's and DMI terms were derived considering linear, single site variations of the magnetic moment, which is sufficient in the case of non-collinear arrangement. In this present work, the non-collinear arrangement is also central, but we have followed an approach of making two site spin rotations for the calculations of interaction parameters of the spin-Hamiltonian.

The comparison between collinear and CP case can be seen in Table 2 and the DMI directions are shown in Fig. 2. The strength of the DMI is seen to be significantly enhanced for the co-planar orientation. It is unlikely that this enhancement is due to spin-orbit coupling, that is expected to influence the electronic structure in a similar way, for any magnetic configuration. Our explanation of this enhancement, presented below, follows instead an analysis of spin currents, that are known to originate from either spin-orbit coupling or a co-planarly aligned magnetism³⁵.

Influence of spin and charge current on the DMI. It is known that non-collinearity can lead to spin and charge currents in a system³⁶. Moreover, the relation between the DMI and spin-current was discussed in Refs.³⁷ and³⁸. The spin-current that flows between a pair of atoms that the DMI couples, is the main reason for the difference between the collinear and NC DMI strengths. Also, since both the collinear and the CP Néel state have no scalar spin chirality, i.e. $C_{123} = \mathbf{S}_1 \cdot (\mathbf{S}_2 \times \mathbf{S}_3) = 0$, the charge-current flowing in the system is weak and is exclusively due to the spin-orbit coupling³⁶. These mechanisms have been recently discussed in Ref.³⁹.

In order to analyze in detail the role of the spin and charge currents for the DMI, we first divide the Green's function (GF) into spin independent \underline{G}_{ij}^0 and spin dependent \underline{G}_{ij}^μ parts. Here $\mu = x, y, z$ and \underline{G}_{ij} being 9×9 matrices in case of *spd*-orbitals, with orbital indexes written here as α, β when needed explicitly as $G_{ij\alpha\beta}$. In this representation, one can describe the behaviour of the GF under a given symmetry operation T , that is an operator that transposes simultaneously the orbital and site indices. As discussed previously³², one can further decompose the GF as

$$\underline{G}_{ij}^0 = \underline{G}_{ij}^{00} + \underline{G}_{ij}^{01} \quad (4)$$

and

$$\underline{G}_{ij}^\mu = \underline{G}_{ij}^{\mu 0} + \underline{G}_{ij}^{\mu 1}, \quad (5)$$

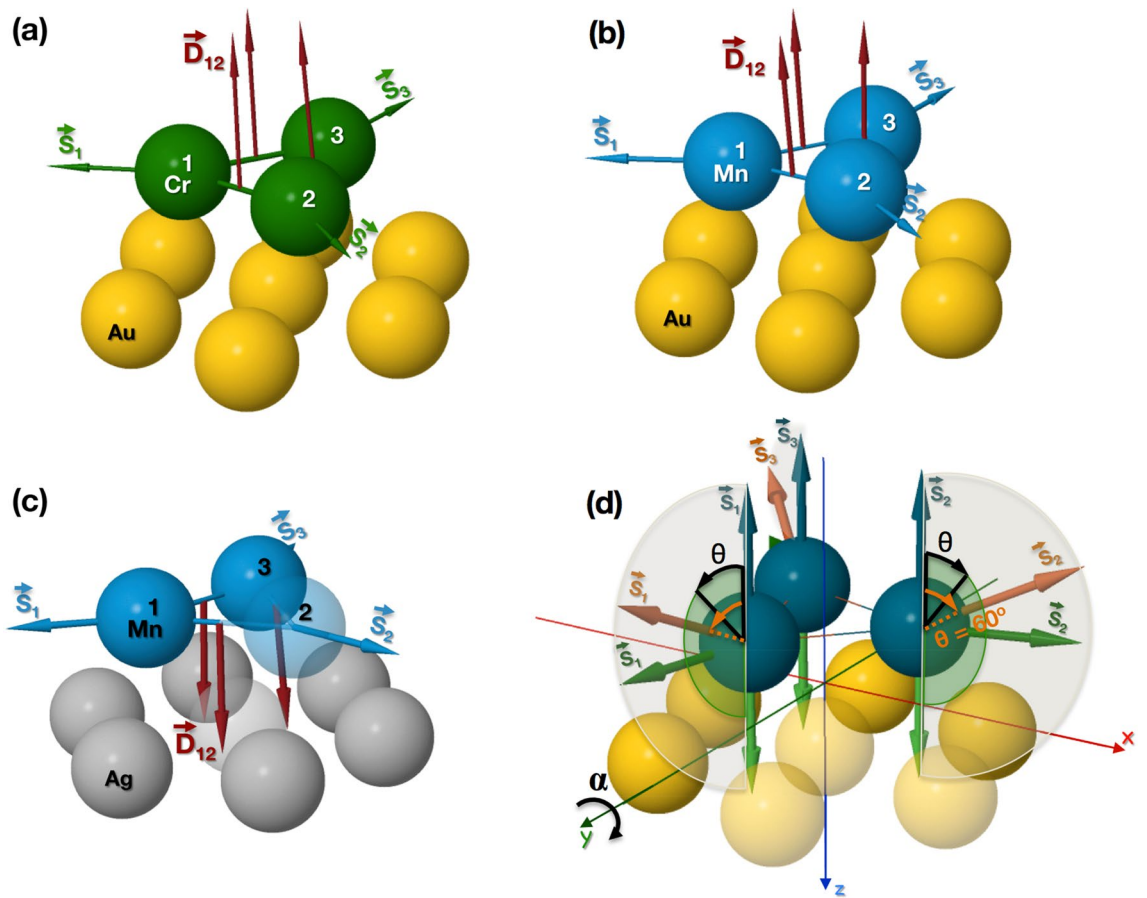


Figure 2. Schematic representation of a triangular trimer of: (a) Cr on Au(111), (b) Mn on Au(111) fcc and (c) Mn on Ag(111) fcc surfaces. The dark red arrows denote the DMI directions (\mathbf{D}_{ij}), in case of NC magnetic configuration (Néel type state), and they are positioned in-between two atoms which the interaction corresponds to. (d) Diagram with the different magnetic configurations used in the DMI calculations as a function of the θ and α angles.

where the second index, introduced in Eqs. (4) and (5), denotes whether that part of the GF is even (0) or odd (1) under T . This property is valid for a real basis, in case of spherical harmonics. Further details of this derivation can be seen in Ref.³². The definition of the components of the GFs in Eqs. (4) and (5) imply that

$$\left(G_{ij\alpha\beta}^{00}\right)^T = G_{ji\beta\alpha}^{00} = G_{ij\alpha\beta}^{00}, \tag{6}$$

and

$$\left(G_{ij\alpha\beta}^{01}\right)^T = G_{ji\beta\alpha}^{01} = -G_{ij\alpha\beta}^{01}. \tag{7}$$

Furthermore, the two-index formalism can be obtained with the one-index formalism from the relationship

$$\underline{G}_{ij}^0 + \underline{G}_{ij}^{0T} = 2\underline{G}_{ij}^{00} \tag{8}$$

$$\underline{G}_{ij}^0 - \underline{G}_{ij}^{0T} = 2\underline{G}_{ij}^{01}. \tag{9}$$

The four different parts of the decomposed Green function have direct physical connections³², as tabulated below.

\underline{G}^{00}	Charge density
\underline{G}^{01}	Charge current
$\underline{G}^{\mu 0}$	Spin density
$\underline{G}^{\mu 1}$	Spin current

With these relationships, one can rewrite the DMI formula, Eq. (35) from the “Methods” section, as

$$D_{ij}^{\mu} = \frac{1}{2\pi} \Re \int \text{Tr} \left\{ \delta_i \underline{G}_{ij}^{00} \delta_j \underline{G}_{ji}^{\mu 1} + \delta_i \underline{G}_{ij}^{01} \delta_j \underline{G}_{ji}^{\mu 0} \right\} = \left(D_{ij}^S + D_{ij}^C \right)^{\mu}. \quad (10)$$

While \underline{G}^{00} and $\underline{G}^{\mu 0}$ are the result of the magnetic system, \underline{G}^{01} and $\underline{G}^{\mu 1}$ are connected with spontaneous currents that may result from the NC magnetic texture of the system. We will exemplify these mechanism later in the paper. With this formulation, one may divide the DMI in two parts: one related with the spin-current, called $D^S \propto \underline{G}^{\mu 1}$; and other one related with the charge-current $D^C \propto \underline{G}^{01}$. In this interpretation of the DMI, its origin is due to inter-atomic spin and charge currents.

The origin and the mechanism behind the DMI has been intensively discussed in the literature^{34,36–38,40}. The DMI is known to be a direct effect from the broken inversion symmetry, caused by the SOC. In the case analyzed here, a triangle trimer, if the magnetic configuration is collinear, e.g. with the magnetic moments aligned parallel to the surface normal, the SOC induces a current that has direct influence on the DMI. If one turns off the SOC (see Computational details Section), of this collinear structure, both spin and charge currents vanish, due to the lack of both vector and scalar spin chiralities. However, there are other mechanisms which induce spin and charge currents into a system. The non-collinearity is the relevant mechanism of the presently analyzed systems, from which an additional current flows. Therefore, the currents that may flow in the systems analyzed here, has two different sources which will affect differently the DMI. The electronic structure method used here allows to scale the spin-orbit strength and it is therefore possible to analyse the relative importance of relativistic effects, and the influence of NC magnetic moments. Our results show that in the absence of SOC, the current driven by the non-collinearity is large, with the result that a significant DMI appears, even in the absence of SOC. This has recently also been discussed for Mn_3Sn ³². A different perspective of these ideas, based on multi-spin and/or multi-scale interaction has recently been discussed by Brinker et al in Ref.⁴¹. Efforts have been made trying to map a many-body problem onto spin-lattice models attempting to take in consideration the multi-site spin-interaction and their origins^{42–44}. The model used in this paper only considers terms up to second order, meaning that high-order terms are folded into the terms here presented. We suggest then that non-collinear exchange interactions are incorporated into our DMI-like term.

In this work, we have performed calculations of the DMI for three different trimers with different magnetic configurations, as represented in Fig. 2d, namely: (i) a rotation of the magnetic moments from a ferromagnetic configuration to a CP Néel magnetic structure and back to a ferromagnetic configuration. This is achieved by rotating the out of plane component of each atomic moment from $\theta = 0^\circ$ to 180° (data shown from $\theta = 60^\circ$ to 120°), while keeping the in-plane component of each magnetic moment at a 120° with respect to the neighbouring Mn (or Cr) atom. We also performed calculations (ii) of the DMI while scaling of the SOC strength, for a configuration when the magnetic moments have an in-plane angle of 120° between each other and an angle of 60° with respect to the z -axis ($\theta = 60^\circ$). Furthermore, we investigated the effects of a global spin rotation, R_α , of the magnetic configuration around the y axis with an angle α (iii). Once the rotation is done, the new DMI was calculated and the vectors were rotated back to the original reference frame.

In Fig. 3, case (i), we show results from a calculation of the DMI for the triangular trimers of Cr on Au(111), Mn on Au(111) and Mn on Ag(111) at every 10° , starting from an out-of plane angle of the moment (θ) of 60° and ending at 120° . A self consistent calculation for the electronic structure was done for every step, and the DMI was evaluated. The calculations were done including SOC (full line) and without SOC (dashed line), and it was found that in general the difference between the two calculations is minor. Our results also show that if the magnetic configuration is collinear, the DMI only exists in the presence of the SOC (data not shown in Fig. 3). However, in the NC magnetic configuration case, the DMI is clearly seen from the figure to be non-zero even in the absence of the SOC. This is due to the spin- and charge currents flowing in the system, that are driven by the non-collinearity. Note that Fig. 3 describes the strength of the three components of the Dzyaloshinskii-Moriya interaction. It is noteworthy that when $\theta = 90^\circ$, i.e. the Néel magnetic structure, the scalar spin chirality C_{123} is zero and the charge current flowing in the system is zero. This means that the charge-current dependent part of the DMI, D^C , vanishes and all the contribution comes from the spin-current dependent D^S , whose z components are allowed by symmetry. Finally, in the CP Néel state and in the lack of SOC, the x and y components of the spin-current dependent part of DMI are also zero.

In Fig. 4, case (ii), we show results from a converged calculation, with the magnetic moments having an angle of $\theta = 60^\circ$ with respect to the z -axis. In this plot we show results of the x -, y - and z -components of the DMI as function of a scaling parameter that was used to tune the strength of the SOC. In this plot, a value of 1 on the abscissa means 100% of the true, calculated SOC strength, and e.g. a value 0.5 corresponds to 50% of the true, calculated SOC strength. One may note from the figure that for the particular configurations considered, the influence of the SOC is fairly minimal. This demonstrates that the DMI can have a huge, non-relativistic source, that emanates from currents driven by the non-collinearity of the magnetism.

In Fig. 5, case (iii), the set-up of Fig. 4 is repeated with $\theta = 60^\circ$, but now a global spin rotation, R_α , of the magnetic moment around the y -axis is done. Here, α is the varied angle that is used to rotate moments around the y -axis (see Fig. 2d). The non-relativistic part of the DMI should be a constant and therefore, for zero SOC one expects $\mathbf{D}_{ij}(\alpha) \cdot R_\alpha \hat{e}_i \times R_\alpha \hat{e}_j = \mathbf{D}_{ij}(0) \cdot \hat{e}_i \times \hat{e}_j$, for any value of α . In the limit of weak SOC, the quantity $R_\alpha^{-1} \mathbf{D}_{ij}(\alpha) \approx \mathbf{D}_{ij}(0)$ should be fairly independent of α with any anisotropy directly connected to the SOC. It is possible from Fig. 5 to verify an almost constant value for the DMI with very small dependence on α . This corroborates that the DMI is present, in this NC scenario, mostly due to non-relativistic effects, a conclusion also reached in the analysis of Fig. 4.

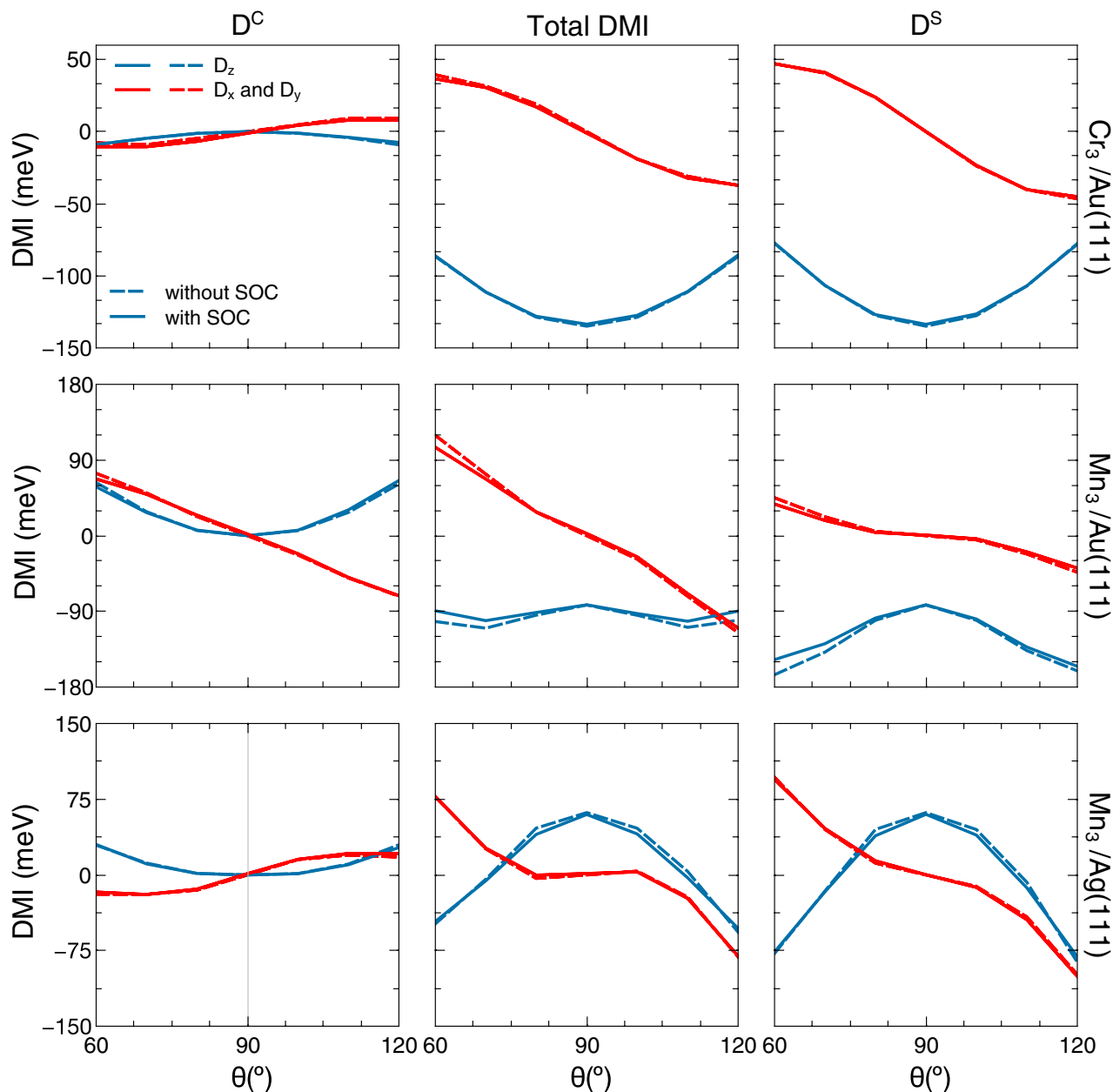


Figure 3. DMI calculated when varying the vertical angle of the magnetic moments between $\theta = 60^\circ$ and $\theta = 120^\circ$. On top we have the plot for Cr triangular trimer on Au(111), middle for the triangular trimer of Mn on Au(111) and on bottom the Mn triangular trimer on Ag(111). On the left panels we show results for the DMI part related with the charge-current (D^C), on the right panels we show data for the spin-current dependent part of the DMI (D^S), and the middle panels contain the total DMI. The blue line denotes the D_z component while the red line denotes the in-plane component as $D_x = D_y = D_{\parallel}/\sqrt{2}$. The full line stands for the calculation when the spin-orbit coupling is included, whereas the dashed line denotes the calculation without spin-orbit coupling.

Conclusions

In this work, we have derived the pairwise energy variation between two atoms, in terms of multiple scattering theory, and mapped these results onto a bi-linear Heisenberg Hamiltonian, in order to explicitly evaluate the antisymmetric exchange-coupling parameter, the Dzyaloshinskii-Moriya interaction, from an implementation in the RS-LMTO-ASA method. The RS-LMTO-ASA method was used to calculate the electronic structure of a Cr triangular trimer on Au(111) surface and Mn triangular trimers on Au(111) and Au(111) surfaces. From these calculations, we have computed the DMI for different magnetic configurations. Firstly, we have found that the DMI evaluated from a ferromagnetic configuration has both strength and direction of the DMI that are in good agreement with previous values found in the literature, when a comparison is possible. Furthermore, we find that, similar to the exchange-coupling parameter, J_{ij} , the DMI can strongly depend on the magnetic configuration. To

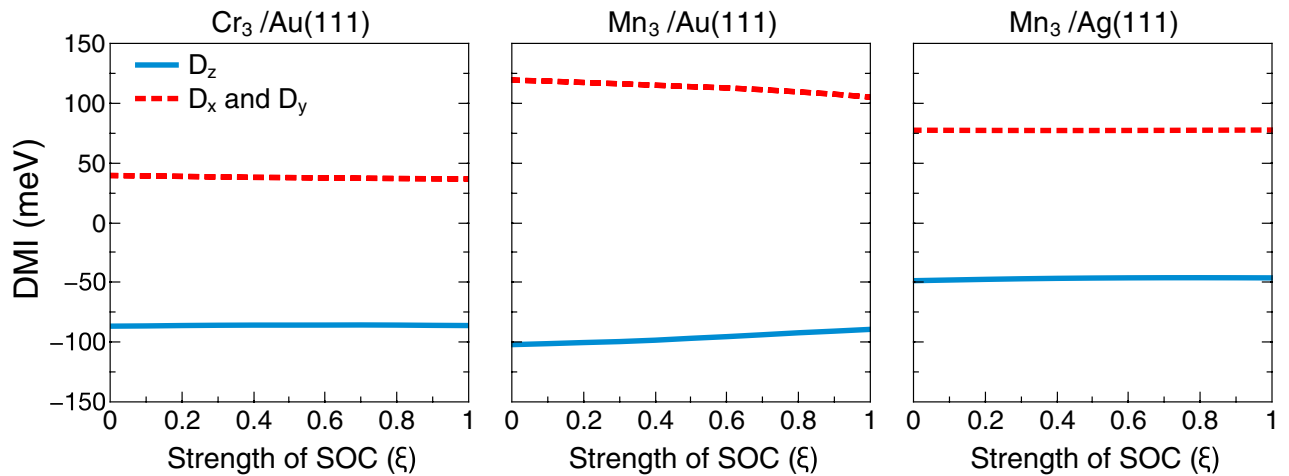


Figure 4. Scaling of the strength of the SOC calculated for a Néel like magnetic structure, with a fixed value of angle between atomic moments and the z-axis $\theta = 60^\circ$. On the left panel we show results for the Cr triangular trimer on Au(111), the middle panel contains results for the triangular trimer of Mn on Au(111) and on the right panel we show data for the Mn triangular trimer on Ag(111). The blue line denotes the D_z component while the red line denotes the in-plane components $D_x = D_y$.

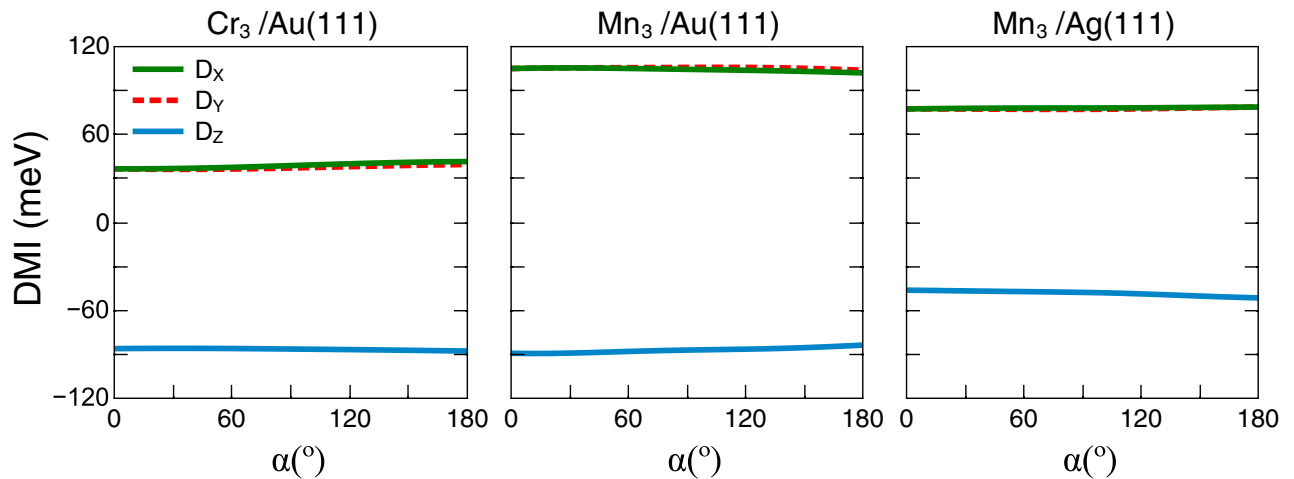


Figure 5. Calculated DMI when a global spin rotation of the magnetic structure by an angle α around the y-axis is performed. On the left panel we show results for the Cr triangular trimer on Au(111), the middle panel contains results for the triangular trimer of Mn on Au(111) and on the right panel we show data for the Mn triangular trimer on Ag(111). The green, (dashed) red, and blue lines denote the D_x , D_y , and D_z components, respectively.

reach this conclusion, the DMI was evaluated from a NC magnetic configuration, for all trimers. The results show a drastic difference, both for the direction and strength of the DMI, between a collinear and a NC configuration.

In addition, we argue here that the DMI carries a dependence on the spin and charge currents flowing in the system, that can be induced by either spin-orbit effects or by a NC magnetic configuration. Thus, the fact that the non-collinearity induces a spin and charge current highly contributes to the final value and direction of the DMI. In the particular case of the triangular trimer and the NC magnetic configuration, we have shown that the DMI is mostly influenced by non-relativistic effects. In fact, the results presented here show that the non-relativistic contribution can be orders of magnitude larger than the contribution from spin-orbit coupling. Lastly, it is noteworthy that this paper describes a simple way of calculating all the three components of the DMI from a single calculation that works for any considered magnetic configuration.

Methods

The fundamental equation of a scalar relativistic multiple scattering theory formalism is given as

$$\left(\tau_{ij}^{-1}\right)_{L\sigma,L'\sigma'} = p_{iL\sigma\sigma'}\delta_{ij}\delta_{LL'} - G_{ij,LL'}^0\delta_{\sigma\sigma'}, \quad (11)$$

where $\underline{\underline{\tau}}_{ij}$ stands for the scattering path operator (SPO), $\underline{\underline{p}}_{\underline{\underline{i}}}$ denotes the inverse of single site scattering operator (ISO). The double underline stands for the fact that they are, in case of spd orbitals (single underline), 18×18 matrices in the spin and orbital (double underline). In Eq. (11) $L = (l, m)$ stands for the angular momentum and magnetic quantum numbers, σ refers to the spin-index, $\underline{\underline{G}}_{ij}^0$ is the free (or bare) electron Green's function and indices i and j refer to the considered lattice sites. $\underline{\underline{G}}_{ij}^0$ is calculated from the Hamiltonian of the free particle, hence it is spin-independent. We introduce a general notation for the single site scattering operator in a NC framework as

$$\underline{\underline{t}}_i = \underline{\underline{t}}_i^0(\varepsilon)I_2 + \underline{\underline{t}}_i(\varepsilon)\mathbf{e}_i\sigma, \tag{12}$$

where the unit vector \mathbf{e}_i refers to the magnetic spin moment at site i (as it was already defined in the Introduction), σ stands for the vector formed by Pauli-matrices, I_2 is the unit matrix in spin space, $\underline{\underline{t}}_i^0$ denotes the non-magnetic (charge) part, and $\underline{\underline{t}}_i$ stands for the magnetic (spin) part of the single site scattering operator, ε is the energy variable.

For the ISO, one can introduce a similar notation as for the $\underline{\underline{t}}_i$ in Eqn. (12) as follows,

$$\underline{\underline{p}}_{\underline{\underline{i}}} = \underline{\underline{p}}_{\underline{\underline{i}}}^{-1} = \underline{\underline{p}}_{\underline{\underline{i}}}^0 I_2 + \underline{\underline{p}}_{\underline{\underline{i}}} \mathbf{e}_i \sigma. \tag{13}$$

Later we will need to deal with the variation of the ISO under a small rotation that can be written as

$$\delta \underline{\underline{p}}_{\underline{\underline{i}}} = \underline{\underline{p}}_{\underline{\underline{i}}} \delta \mathbf{e}_i \sigma, \tag{14}$$

where $\delta \mathbf{e}_i$ stands for the deviation of a spin moment after an infinitesimal rotation at site i . Finally, the SPO has a structure as

$$\underline{\underline{\tau}}_{ij} = \underline{\underline{T}}_{ij}^0 I_2 + \underline{\underline{T}}_{ij} \sigma, \tag{15}$$

where $\underline{\underline{T}}_{ij}^0$ denotes the charge while $\underline{\underline{T}}_{ij} = (\underline{\underline{T}}_{ij}^x, \underline{\underline{T}}_{ij}^y, \underline{\underline{T}}_{ij}^z)$ stands for the spin part of the SPO. We have defined the quantities required to calculate the pairwise total energy (grand potential- Ω) variation in a NC framework, i.e., when a spin at site i and an other spin at site j are rotated by an infinitesimal angle simultaneously. As it has been shown in Ref.²⁶, the expression for changes of the grand potential when spins at site i and j are rotated with infinitesimal angles can be written

$$\delta \Omega_{ij} = -\frac{1}{\pi} \int_{-\infty}^{\varepsilon_F} d\varepsilon \text{Im} \text{Tr}_{\sigma L} \left(\delta \underline{\underline{p}}_{\underline{\underline{i}}} \underline{\underline{\tau}}_{ij} \delta \underline{\underline{p}}_{\underline{\underline{j}}} \underline{\underline{\tau}}_{ji} \right), \tag{16}$$

where both the ISO and the SPO depend on the energy, ε . This expression is commonly evaluated using the Lloyd formula⁴⁵. For this purpose, we introduce the matrix

$$A_{ij}^{\alpha\beta} = \frac{1}{\pi} \int_{-\infty}^{\varepsilon_F} d\varepsilon \text{Im} \text{Tr}_L \left(\underline{\underline{p}}_i \underline{\underline{T}}_{ij}^\alpha \underline{\underline{p}}_j \underline{\underline{T}}_{ji}^\beta \right), \tag{17}$$

and the matrix

$$\hat{A}_{ij}^{\alpha\beta} = \frac{1}{\pi} \int_{-\infty}^{\varepsilon_F} d\varepsilon \text{Re} \text{Tr}_L \left(\underline{\underline{p}}_i \underline{\underline{T}}_{ij}^\alpha \underline{\underline{p}}_j \underline{\underline{T}}_{ji}^\beta \right). \tag{18}$$

Inserting Eqs. (14) and (15) into Eqn. (16), and using Eq. (17), one can formally obtain that

$$\delta \Omega_{ij} = -2J_{ij}^* \delta \mathbf{e}_i \delta \mathbf{e}_j - 4 \sum_{\mu, \nu=x,y,z} \delta e_i^\mu A_{ij}^{\mu\nu} \delta e_j^\nu - 2D_{ij}^{*\mu} (\delta \mathbf{e}_i \times \delta \mathbf{e}_j), \tag{19}$$

where expression

$$J_{ij}^* = A_{ij}^{00} - \sum_{\mu=x,y,z} A_{ij}^{\mu\mu} \tag{20}$$

and

$$D_{ij}^{*\mu} = \hat{A}_{ij}^{0\mu} - \hat{A}_{ij}^{\mu 0} \tag{21}$$

have been introduced. The first term in Eq. (19) is denoted $\delta \Omega_{ij}^H$ (for Heisenberg like contributions) while the third term is denoted $\delta \Omega_{ij}^{DM}$ (for DMI like contributions). Here, the new superscript $*$ was introduced in order to differentiate the terms derived from the multiple scattering theory from the ones presented in Eq. (1). However, a practical calculation of exchange parameters used in an effective spin-Hamiltonian, amount to identifying the connection between the parameters in Eq. (1) and those in Eqs. (20) and (21).

We analyse in this paragraph the case when the atomic moments are in a collinear arrangement (and the spin orbit-interaction is absent). One can then write that $\underline{T}_{ij} = (0, 0, T_{ij}^z)$, and the component of the SPO for the up and down spin channels can be defined as $\underline{T}_{ij}^\uparrow = T_{ij}^0 + T_{ij}^z$ while $\underline{T}_{ij}^\downarrow = T_{ij}^0 - T_{ij}^z$. It can be shown that $D_{ij}^{*\mu} = 0$ in this case and the second term in Eq. (19) gives only higher (fourth) order contribution to Ω in terms of the angle variation. Only the first term is left in which J_{ij}^* is simplified to

$$J_{ij}^* = A_{ij}^{00} - A_{ij}^{zz} = A_{ij}^{\uparrow\downarrow}. \tag{22}$$

The expression defined in Eq. (22) is widely used for ab-initio calculations of Heisenberg exchange, and is commonly referred to as the LKAG formula.

In the rest of the section, we analyse for a general NC magnetic configuration what contributions are added to the variation of Ω , when the SOC is considered as a perturbation, i.e. only the terms that being of first order in the SOC parameter, ξ , are kept. One can then write that

$$\delta\Omega'_{ij} = -\frac{1}{\pi} \int_{-\infty}^{\epsilon_F} d\epsilon \text{Im} Tr_{\sigma L} \left(\delta \underline{p}'_{\underline{i}=\underline{j}} \tau'_{\underline{j}=\underline{j}i} \right), \tag{23}$$

where the perturbed quantities are denoted by the symbol \prime . Our task now is to determine the $\delta \underline{p}'$ -s and τ' -s. First, we determined the perturbed single scattering matrix with the help of perturbed Green function. Next, we introduce the perturbed \underline{G}'_{ij} where $\underline{G}'_{ij} = \underline{G}_{ij}^0 + \Delta \underline{G}_{ij}$. The matrix \underline{G}_{ij}^0 has the structure of $\underline{G}_{ij}^0 I_2$, while $\Delta \underline{G}_{ij}$ can be written as $\xi \underline{\Gamma}_{ij} \sigma$, where its vector component $\underline{\Gamma}_{ij}^\mu$ ($\mu = x, y$ and z) is obtained as

$$\underline{\Gamma}_{ij}^\mu = \sum_k \underline{G}_{ik}^0 \underline{L}^\mu \underline{G}_{kj}^0, \tag{24}$$

and where \underline{L}^μ is a component of the angular momentum operator. This implies that $\underline{\Gamma}_{ij}$ transforms under T as

$$\left(\underline{\Gamma}_{ij}^\mu \right)^T = -\underline{\Gamma}_{ji}^\mu. \tag{25}$$

Keeping the leading terms, we get that $\underline{t}'_i = \underline{t}_i + \xi \underline{t}_i (\underline{\Gamma}_{ii} \sigma) \underline{t}_i$ which can alternatively be written as $\underline{t}'_i = \underline{t}_i (\underline{I} + \xi (\underline{\Gamma}_{ii} \sigma) \underline{t}_i)$ where \underline{I} is the unit matrix. Then $\left(\underline{t}'_i \right)^{-1} = \underline{t}_i^{-1} - \xi (\underline{\Gamma}_{ii} \sigma)$ and

$$\underline{p}'_{\underline{i}} \simeq \underline{p}_{\underline{i}} - \xi (\underline{\Gamma}_{ii} \sigma) = \underline{p}_{\underline{i}}^0 + \left(\underline{p}_{\underline{i}} \mathbf{e}_i - \xi \underline{\Gamma}_{ii} \right) \sigma, \tag{26}$$

see Eqs. (12–13). This implies that

$$\delta \underline{p}'_{\underline{i}} \simeq \underline{p}_{\underline{i}} \delta \mathbf{e}_i \sigma = \delta \underline{p}_{\underline{i}}, \tag{27}$$

i.e., we have to calculate the simpler expression

$$\delta\Omega'_{ij} \simeq -\frac{1}{\pi} \int_{-\infty}^{\epsilon_F} d\epsilon \text{Im} Tr_{\sigma L} \left(\delta \underline{p}_{\underline{i}=\underline{j}} \tau'_{\underline{j}=\underline{j}i} \right) \tag{28}$$

that contains the perturbed SPO, however, the ISO is present in a non-perturbed form.

Next we need to determine the perturbed SPO. It can be shown that

$$\underline{\tau}'_{ij} = \underline{\tau}_{ij} + \Delta \underline{\tau}_{ij}, \tag{29}$$

where

$$\Delta \underline{\tau}_{ij} = \xi \underline{t}_i (\underline{\Gamma}_{ii} \sigma) \underline{t}_i \delta_{ij} + \xi \underline{t}_i (\underline{\Gamma}_{ii} \sigma) \underline{t}_i \underline{G}_{ij}^0 \underline{t}_j + \xi \underline{t}_i \underline{G}_{ij}^0 \underline{t}_j (\underline{\Gamma}_{jj} \sigma) \underline{t}_j + \xi \underline{t}_i (\underline{\Gamma}_{ij} \sigma) \underline{t}_j. \tag{30}$$

It can furthermore be demonstrated that $\Delta \underline{\tau}_{ij}$ has the same structure as $\underline{\tau}_{ij}$, i.e.,

$$\Delta \underline{\tau}_{ij} = \Delta T_{ij}^0 I_2 + \Delta \underline{T}_{ij} \sigma. \tag{31}$$

Using Eqs. (24) and (30), it can be shown by using Eq. (25) that

$$\left(\Delta \underline{T}_{ij}^\alpha \right)^T = -\Delta \underline{T}_{ji}^\alpha, \tag{32}$$

where α runs over the 0, x, y and z. This implies that

$$Tr_L \left(\underline{p}_i \Delta \underline{T}_{ij}^\alpha \underline{p}_j \underline{T}_{ji}^\beta \right) = -Tr_L \left(\underline{p}_i \underline{T}_{ij}^\beta \underline{p}_j \Delta \underline{T}_{ji}^\alpha \right) \tag{33}$$

and

$$\text{Tr}_L(\underline{p}_i T_{ij}^\alpha \underline{p}_j \Delta T_{ji}^\beta) = -\text{Tr}_L(\underline{p}_i \Delta T_{ij}^\beta \underline{p}_j T_{ji}^\alpha). \quad (34)$$

Next, we define the matrices $A_{ij}^{\alpha\beta}$ and $\hat{A}_{ij}^{\alpha\beta}$ as follows: we replace T_{ij}^α by $\underline{T}_{ij}^\alpha$ and T_{ji}^β by \underline{T}_{ji}^β in Eqs. (17) and (18), respectively, where $\underline{T}_{ij}^\alpha = T_{ij}^\alpha + \Delta T_{ij}^\alpha$ and $\underline{T}_{ji}^\beta = T_{ji}^\beta + \Delta T_{ji}^\beta$. Finally, we define \mathbf{D}_{ij}^* as follows,

$$D_{ij}^{*\mu} = \hat{A}_{ij}^{0\mu} - \hat{A}_{ij}^{\mu 0}. \quad (35)$$

By using these definitions, we get from Eq. (28) that

$$\delta\Omega'_{ij} = -2 \left(A_{ij}^{00} - \sum_{\mu=x,y,z} A_{ij}^{\mu\mu} \right) \delta\mathbf{e}_i \delta\mathbf{e}_j - 2 \sum_{\mu,\nu=x,y,z} \delta e_i^\mu (A_{ij}^{\mu\nu} + A_{ij}^{\nu\mu}) \delta e_j^\nu - 2\mathbf{D}_{ij}^* (\delta\mathbf{e}_i \times \delta\mathbf{e}_j), \quad (36)$$

where $A_{ij}^{\alpha\beta} \neq A_{ij}^{\beta\alpha}$. However, by using Eqs. (33) and (34), it can be shown that $A_{ij}^{\alpha\alpha} = A_{ij}^{\alpha\alpha}$. In addition, by using the same equations, it can be also written that $A_{ij}^{\mu\nu} + A_{ij}^{\nu\mu} = 2A_{ij}^{\mu\nu}$. This implies that Eq. (36) will be reduced to the expression

$$\delta\Omega'_{ij} = -2J_{ij}^* \delta\mathbf{e}_i \delta\mathbf{e}_j - 4 \sum_{\mu,\nu=x,y,z} \delta e_i^\mu A_{ij}^{\mu\nu} \delta e_j^\nu - 2\mathbf{D}_{ij}^* (\delta\mathbf{e}_i \times \delta\mathbf{e}_j). \quad (37)$$

From this expression we note that primed quantities, that signify that they contain linear contributions of the SOC, are only found for the DMI interaction. Hence, we conclude from perturbation theory that spin-orbit interaction influences only the DMI interaction.

Summarizing the “Methods” section, we have shown that the exchange parameter J_{ij} defined in the spin model, Eq. (1), can be mapped onto J_{ij}^* given by Eq. (20) for a general, NC, spin arrangement. Note that the mapping is correct if the second term in Eq. (19) is not relevant. This is the case for instance with symmetry resolved exchange parameter in the T_{2g} channel in bcc Fe bulk²⁵. We can also note that the J_{ij} parameter in Eq. (1) for collinear magnets is the LKAG parameter given by Eq. (22). In addition, we have shown that the DMI vector \mathbf{D}_{ij} can be calculated from the electronic structure by the \mathbf{D}_{ij}^* formula given by Eq. (21). This formula is general, and holds for any kind of NC spin configuration. We have also shown, see Eq. (37) that the SOC interaction contributes only to the DMI interaction in leading order.

Computational details. The calculations were performed using the ab initio RS-LMTO-ASA method^{46–52}, which is suitable to describe the physics of isolated clusters supported on surfaces in an efficient way, since it is real-space based and does not depend on translational symmetry. Moreover, the RS-LMTO-ASA method has been generalized to describe NC magnetism^{46,49,53}, and is based on the Haydock recursion method⁵⁴. Our Hamiltonians are constructed within an RS-LMTO-ASA formalism⁵⁵, and therefore, all calculations presented here are fully self-consistent, and the spin densities were treated within the local spin-density approximation (LSDA)⁵⁶. The continued fraction, that occurs in recursion method, have been terminated with the Beer-Pettifor terminator⁵⁷ after 21 recursion levels. The electronic structure calculations were also performed using the ASA and the full potential approximation (latter not shown) and no distinguished differences were seen that would change the conclusions of the paper. The spin-orbit coupling interaction is treated by adding a $H_{SOC} = \xi \mathbf{L} \cdot \mathbf{S}$ to the Kohn-Sham Hamiltonian, with ξ calculated self-consistently. When calculations without SOC are mentioned in the text, it means that we take $\xi \rightarrow 0$ after the self-consistent calculation is done.

Received: 3 July 2020; Accepted: 2 November 2020

Published online: 23 November 2020

References

1. Heinze, S. *et al.* Spontaneous atomic-scale magnetic skyrmion lattice in two dimensions. *Nat. Phys.* **7**, 713–718. <https://doi.org/10.1038/nphys2045> (2011).
2. Pereira, M. *et al.* Topological excitations in a kagome magnet. *Nat. Commun.* **5**, 4815. <https://doi.org/10.1038/ncomms5815> (2014).
3. Fert, A., Reyren, N. & Cros, V. Magnetic skyrmions: Advances in physics and potential applications. *Nat. Rev. Mater.* **2**, 1–15. <https://doi.org/10.1038/natrevmats.2017.31> (2017).
4. Hoshino, S. & Nagaosa, N. Theory of the magnetic skyrmion glass. *Phys. Rev. B* **97**, 024413. <https://doi.org/10.1103/PhysRevB.97.024413> (2018).
5. Zhang, Y. *et al.* Magnetic skyrmions without the skyrmion Hall effect in a magnetic nanotrack with perpendicular anisotropy. *Nanoscale* **9**, 10212–10218. <https://doi.org/10.1039/C7NR01980G> (2017).
6. Maccariello, D. *et al.* Electrical detection of single magnetic skyrmions in metallic multilayers at room temperature. *Nat. Nanotech.* **13**, 233–237. <https://doi.org/10.1038/s41565-017-0044-4> (2018).
7. Seaberg, M. H. *et al.* Nanosecond X-ray photon correlation spectroscopy on magnetic skyrmions. *Phys. Rev. Lett.* **119**, 067403. <https://doi.org/10.1103/PhysRevLett.119.067403> (2017).
8. Matsumoto, T., So, Y.-G., Kohno, Y., Ikuhara, Y. & Shibata, N. Stable magnetic skyrmion states at room temperature confined to corrals of artificial surface pits fabricated by a focused electron beam. *Nano Lett.* <https://doi.org/10.1021/acs.nanolett.7b03967> (2018).
9. Jalil, M. B. A. *et al.* Stability of topological charge of magnetic skyrmion configurations. *J. Magnet. Magnet. Mater.* **399**, 155–158. <https://doi.org/10.1016/j.jmmm.2015.09.064> (2016).

10. Dzyaloshinsky, I. A thermodynamic theory of “weak” ferromagnetism of antiferromagnetics. *J. Phys. Chem. Solids* **4**, 241–255. [https://doi.org/10.1016/0022-3697\(58\)90076-3](https://doi.org/10.1016/0022-3697(58)90076-3) (1958).
11. Udvardi, L., Szunyogh, L., Palotás, K. & Weinberger, P. First-principles relativistic study of spin waves in thin magnetic films. *Phys. Rev. B* **68**, 104436. <https://doi.org/10.1103/PhysRevB.68.104436> (2003).
12. Moriya, T. Anisotropic superexchange interaction and weak ferromagnetism. *Phys. Rev.* **120**, 91–98. <https://doi.org/10.1103/PhysRev.120.91> (1960).
13. Crépeux, A. & Lacroix, C. Dzyaloshinsky-Moriya interactions induced by symmetry breaking at a surface. *J. Magnet. Magnet. Mater.* **182**, 341–349. [https://doi.org/10.1016/S0304-8853\(97\)01044-5](https://doi.org/10.1016/S0304-8853(97)01044-5) (1998).
14. Antal, A. *et al.* First-principles calculations of spin interactions and the magnetic ground states of Cr trimers on Au(111). *Phys. Rev. B* **77**, 174429. <https://doi.org/10.1103/PhysRevB.77.174429> (2008).
15. Udvardi, L. & Szunyogh, L. Chiral asymmetry of the spin-wave spectra in ultrathin magnetic films. *Phys. Rev. Lett.* **102**, 207204. <https://doi.org/10.1103/PhysRevLett.102.207204> (2009).
16. Skubic, B., Hellsvik, J., Nordström, L. & Eriksson, O. A method for atomistic spin dynamics simulations: Implementation and examples. *J. Phys.: Condens. Matter* **20**, 315203. <https://doi.org/10.1088/0953-8984/20/31/315203> (2008).
17. Nyquist, H. Thermal agitation of electric charge in conductors. *Phys. Rev.* **32**, 110–113. <https://doi.org/10.1103/PhysRev.32.110> (1928).
18. Chandler, D. *Introduction to Modern Statistical Mechanics* (Oxford University Press, Oxford, 1987).
19. Söderlind, P. *et al.* Prediction of the new efficient permanent magnet SmCoNiFe 3. *Phys. Rev. B* **96**, 100404. <https://doi.org/10.1103/PhysRevB.96.100404> (2017).
20. Chimata, R. *et al.* Magnetism and ultrafast magnetization dynamics of Co and CoMn alloys at finite temperature. *Phys. Rev. B* **95**, 214417. <https://doi.org/10.1103/PhysRevB.95.214417> (2017).
21. Keshavarz, S. *et al.* Exchange interactions of CaMnO₃ in the bulk and at the surface. *Phys. Rev. B* **95**, 115120. <https://doi.org/10.1103/PhysRevB.95.115120> (2017).
22. Locht, I. L. M. *et al.* Standard model of the rare earths analyzed from the Hubbard I approximation. *Phys. Rev. B* **94**, 085137. <https://doi.org/10.1103/PhysRevB.94.085137> (2016).
23. Yadav, R. *et al.* Heavy-mass magnetic modes in pyrochlore iridates due to dominant Dzyaloshinskii-Moriya interaction. *Phys. Rev. Mater.* **2**, 074408. <https://doi.org/10.1103/PhysRevMaterials.2.074408> (2018).
24. Koumpouras, K. *et al.* A majority gate with chiral magnetic solitons. *J. Phys.: Condens. Matter* **30**, 375801. <https://doi.org/10.1088/1361-648X/aad82f> (2018).
25. Szilva, A. *et al.* Theory of noncollinear interactions beyond Heisenberg exchange: Applications to bcc Fe. *Phys. Rev. B* **96**, 144413. <https://doi.org/10.1103/PhysRevB.96.144413> (2017).
26. Szilva, A. *et al.* Interatomic exchange interactions for finite-temperature magnetism and nonequilibrium spin dynamics. *Phys. Rev. Lett.* **111**, 127204. <https://doi.org/10.1103/PhysRevLett.111.127204> (2013).
27. Rodrigues, D. C. M. *et al.* Finite-temperature interatomic exchange and magnon softening in Fe overlayers on Ir(001). *Phys. Rev. B* **94**, 014413. <https://doi.org/10.1103/PhysRevB.94.014413> (2016).
28. Liechtenstein, A. I., Katsnelson, M. I., Antropov, V. P. & Gubanov, V. A. Local spin density functional approach to the theory of exchange interactions in ferromagnetic metals and alloys. *J. Magnet. Magnet. Mater.* **67**, 65–74. [https://doi.org/10.1016/0304-8853\(87\)90721-9](https://doi.org/10.1016/0304-8853(87)90721-9) (1987).
29. Frota-Pessôa, S. Magnetic behavior of 3 d impurities in Cu, Ag, and Au: First-principles calculations of orbital moments. *Phys. Rev. B* **69**, 104401. <https://doi.org/10.1103/PhysRevB.69.104401> (2004).
30. Gubanov, V., Likhtheinstein, A. & Postnikov, A. *Magnetism and the Electronic Structure of Crystals. Lecture Notes in Medical Informatics* (Springer, 1992).
31. Antropov, V., Katsnelson, M. & Liechtenstein, A. Exchange interactions in magnets. *Phys. B: Condens. Matter* **237–238**, 336–340. [https://doi.org/10.1016/S0921-4526\(97\)00203-2](https://doi.org/10.1016/S0921-4526(97)00203-2) (1997). Proceedings of the Yamada Conference XLV, the International Conference on the Physics of Transition Metals.
32. Cardias, R. *et al.* Dzyaloshinskii-Moriya interaction in absence of spin-orbit coupling. [arXiv:2003.04680](https://arxiv.org/abs/2003.04680) [cond-mat] (2020).
33. Katsnelson, M. I. & Liechtenstein, A. I. First-principles calculations of magnetic interactions in correlated systems. *Phys. Rev. B* **61**, 8906–8912. <https://doi.org/10.1103/PhysRevB.61.8906> (2000).
34. Belabbes, A., Bihlmayer, G., Bechstedt, F., Blügel, S. & Manchon, A. Hund’s rule-driven Dzyaloshinskii-Moriya interaction at 3 d-5 d interfaces. *Phys. Rev. Lett.* **117**, 247202. <https://doi.org/10.1103/PhysRevLett.117.247202> (2016).
35. Nordström, L. & Singh, D. J. Noncollinear intra-atomic magnetism. *Phys. Rev. Lett.* **76**, 4420–4423. <https://doi.org/10.1103/PhysRevLett.76.4420> (1996).
36. dos Santos Dias, M., Bouaziz, J., Bouhassoune, M., Blügel, S. & Lounis, S. Chirality-driven orbital magnetic moments as a new probe for topological magnetic structures. *Nat. Commun.* **7**, 13613. <https://doi.org/10.1038/ncomms13613> (2016).
37. Kikuchi, T., Koretsune, T., Arita, R. & Tatara, G. Dzyaloshinskii-Moriya interaction as a consequence of a Doppler shift due to spin-orbit-induced intrinsic spin current. *Phys. Rev. Lett.* **116**, 247201. <https://doi.org/10.1103/PhysRevLett.116.247201> (2016).
38. Freimuth, F., Blügel, S. & Mokrousov, Y. Relation of the Dzyaloshinskii-Moriya interaction to spin currents and to the spin-orbit field. *Phys. Rev. B* **96**, 054403. <https://doi.org/10.1103/PhysRevB.96.054403> (2017).
39. Zhang, Y., Železný, J., Sun, Y., van den Brink, J. & Yan, B. Spin Hall effect emerging from a noncollinear magnetic lattice without spin-orbit coupling. *New J. Phys.* **20**, 073028. <https://doi.org/10.1088/1367-2630/aad1eb> (2018).
40. Karnad, G. V. *et al.* Modification of Dzyaloshinskii-Moriya-interaction-stabilized domain wall chirality by driving currents. *Phys. Rev. Lett.* **121**, 147203. <https://doi.org/10.1103/PhysRevLett.121.147203> (2018).
41. Brinker, S., Dias, M. d. S. & Lounis, S. Prospecting chiral multi-site interactions in prototypical magnetic systems. [arXiv:2004.11110](https://arxiv.org/abs/2004.11110) [cond-mat] (2020).
42. Lászlóffy, A., Rózsa, L., Palotás, K., Udvardi, L. & Szunyogh, L. Magnetic structure of monatomic Fe chains on re(0001): Emergence of chiral multispin interactions. *Phys. Rev. B* **99**, 184430. <https://doi.org/10.1103/PhysRevB.99.184430> (2019).
43. Mankovsky, S., Polesya, S. & Ebert, H. Extension of the standard heisenberg hamiltonian to multispin exchange interactions. *Phys. Rev. B* **101**, 174401. <https://doi.org/10.1103/PhysRevB.101.174401> (2020).
44. Grytsiuk, S. *et al.* Topological-chiral magnetic interactions driven by emergent orbital magnetism. *Nat. Commun.* **11**, 511. <https://doi.org/10.1038/s41467-019-14030-3> (2020).
45. Lloyd, P. Wave propagation through an assembly of spheres: II. The density of single-particle eigenstates. *Proc. Phys. Soc.* **90**, 207–216. <https://doi.org/10.1088/0370-1328/90/1/323> (1967).
46. Frota-Pessôa, S. First-principles real-space linear-muffin-tin-orbital calculations of 3 d impurities in Cu. *Phys. Rev. B* **46**, 14570–14577. <https://doi.org/10.1103/PhysRevB.46.14570> (1992).
47. Klautau, A. B. & Frota-Pessôa, S. Orbital moments of 3d adatoms and Co nanostructures on Cu(001) surfaces. *Surf. Sci.* **579**, 27–36. <https://doi.org/10.1016/j.susc.2005.01.032> (2005).
48. Bergman, A., Nordström, L., Burlamaqui Klautau, A., Frota-Pessôa, S. & Eriksson, O. Magnetic interactions of Mn clusters supported on Cu. *Phys. Rev. B* **73**, 174434. <https://doi.org/10.1103/PhysRevB.73.174434> (2006).
49. Bergman, A., Nordström, L., Burlamaqui Klautau, A., Frota-Pessôa, S. & Eriksson, O. Magnetic structures of small Fe, Mn, and Cr clusters supported on Cu(111): Noncollinear first-principles calculations. *Phys. Rev. B* **75**, 224425. <https://doi.org/10.1103/PhysRevB.75.224425> (2007).

50. Bezerra-Neto, M. M. *et al.* Complex magnetic structure of clusters and chains of Ni and Fe on Pt(111). *Sci. Rep.* **3**, 3054. <https://doi.org/10.1038/srep03054> (2013).
51. Klautau, A. B. & Frota-Pessôa, S. Magnetic properties of Co nanowires on Cu(001) surfaces. *Phys. Rev. B* **70**, 193407. <https://doi.org/10.1103/PhysRevB.70.193407> (2004).
52. Frota-Pessôa, S., Klautau, A. B. & Legoas, S. B. Influence of interface mixing on the magnetic properties of Ni/Pt multilayers. *Phys. Rev. B* **66**, 132416. <https://doi.org/10.1103/PhysRevB.66.132416> (2002).
53. Bergman, A., Nordström, L., Klautau, A. B., Frota-Pessôa, S. & Eriksson, O. Non-collinear magnetisation of V clusters supported on a Cu (111) surface: Theory. *Surf. Sci.* **600**, 4838–4842. <https://doi.org/10.1016/j.susc.2006.08.004> (2006).
54. Haydock, R. The recursive solution of the Schrodinger equation. in Ehrenreich, H., Seitz, F. & Turnbull, D. (eds.) *Solid State Physics*, Vol. 35, 215–294. [https://doi.org/10.1016/S0081-1947\(08\)60505-6](https://doi.org/10.1016/S0081-1947(08)60505-6) (Academic Press, 1980).
55. Andersen, O. K. Linear methods in band theory. *Phys. Rev. B* **12**, 3060–3083. <https://doi.org/10.1103/PhysRevB.12.3060> (1975).
56. von Barth, U. & Hedin, L. A local exchange-correlation potential for the spin polarized case. I. *J. Phys. C: Solid State Phys.* **5**, 1629–1642. <https://doi.org/10.1088/0022-3719/5/13/012> (1972).
57. Beer, N. & Pettifor, D. G. The recursion method and the estimation of local densities of states. in (Phariseau, P. & Temmerman, W. M. eds.) *The Electronic Structure of Complex Systems*, NATO ASI Series, 769–777. https://doi.org/10.1007/978-1-4613-2405-8_14 (Springer, Boston, 1984).

Acknowledgements

R. C. and A. B. K. acknowledge financial support from CAPES and CNPq, Brazil. The calculations were performed at the computational facilities of the CENAPAD at University of Campinas, SP, Brazil and the Swedish National Infrastructure for Computing (SNIC). O.E. acknowledges support from the Knut and Alice Wallenberg foundation, the foundation for strategic research (SSF), the Swedish Energy Agency (Energimyndigheten), STandUPP and the Swedish Research Council (VR). L.N. and Y.K. also acknowledge the support from VR. Finally, we would like to acknowledge the support from eSENCE. We gratefully acknowledge the constructive feedback of the two referees of this paper, that helped improving on the presentation.

Author contributions

R.C., M.M.B.-N., M.S.R., A.B., A.B.K., and L.N. conceived and designed these studies. L.N., A.Sz., J.F., and Y.K. contributed to the model development. R.C. and A. B. performed the ab initio calculations. The first version of the manuscript was prepared by R.C., A.B.K. and O.E. All authors discussed the results and contributed to preparing the paper.

Funding

Open Access funding provided by Uppsala University.

Competing Interests

The authors declare no competing interests.

Additional information

Correspondence and requests for materials should be addressed to R.C.

Reprints and permissions information is available at www.nature.com/reprints.

Publisher's note Springer Nature remains neutral with regard to jurisdictional claims in published maps and institutional affiliations.



Open Access This article is licensed under a Creative Commons Attribution 4.0 International License, which permits use, sharing, adaptation, distribution and reproduction in any medium or format, as long as you give appropriate credit to the original author(s) and the source, provide a link to the Creative Commons licence, and indicate if changes were made. The images or other third party material in this article are included in the article's Creative Commons licence, unless indicated otherwise in a credit line to the material. If material is not included in the article's Creative Commons licence and your intended use is not permitted by statutory regulation or exceeds the permitted use, you will need to obtain permission directly from the copyright holder. To view a copy of this licence, visit <http://creativecommons.org/licenses/by/4.0/>.

© The Author(s) 2020